



Self-powered photoelectrochemical aptasensor based on AgInS₂@Co/Ni-UiO-66@CDs photoelectrode for estradiol detection

Ruifang Yuan¹ · Xue Zhang² · Xiaodong Xue² · Rui Feng¹ · Yanxia Zhao¹ · Meng Sun¹ · Liangguo Yan¹ · Tao Yan^{1,3} · Qin Wei³

Received: 28 April 2022 / Accepted: 6 July 2022 / Published online: 1 August 2022
© The Author(s), under exclusive licence to Springer-Verlag GmbH Austria, part of Springer Nature 2022

Abstract

A self-powered photoelectrochemical (PEC) aptasensor was constructed to sensitively detect 17 β -estradiol (E₂). Firstly, a reasonable AgInS₂@Co/Ni-UiO-66@Carbon Nanodots (CDs) photoelectrode with excellent photoelectrochemical performance was built by a simple two-step preparation method. The Co and Ni doping markedly improved the activity of UiO-66; the matched energy level of AgInS₂ and Co/Ni-UiO-66 promoted the separation of electron–hole pairs, and the coupling of CDs further enhanced the conductivity and light utilization. Therefore, a steady anode-photocurrent signal output was obtained in 0.0 V bias voltage, providing a reliable photoelectric translating platform for assembling a self-powered PEC aptasensor. The E₂-aptamer was adopted as a recognition unit to enhance the selectivity and sensitivity of the proposed aptasensor. The specific recognition reaction between E₂ and aptamer administering to a raised photocurrent signal and the concentration of E₂ was quantified by counting the fluctuation of the anode-photocurrent signal. The linear response range of the PEC aptasensor was 1.0 \times 10⁻⁵–10 nmol/L, and the detection limit (S/N = 3) was lower than 3.0 fmol/L under optimal conditions. The fabricated aptasensor exhibited admirable selectivity, high sensitivity, rapid response, and wide linear range, demonstrating an extensive application prospect for environmental endocrine disruptor detection.

Keywords Photoelectrochemical aptasensor · Co/Ni-UiO-66 · Modified carbon nanodots · 17 β -estradiol detection · Ternary chalcogenides

Introduction

17 β -estradiol (E₂) could influence the human reproductive system or bring immune deficiency even at trace levels as one of the most potential and strongest estrogen [1, 2]. Currently, various techniques, including liquid chromatography [3], surface-enhanced Raman scattering (SERS) [4], electrochemical sensor [5], fluorescent sensor [6], and immunosensor [7], have been used for E₂ detection. Nevertheless, most

of these methods generally suffered the defects of cumbersome operations and exorbitant equipment and restricted their practical application to some extent. As a result of the continuous innovation of environmental detection requirements, it is urgently needed to explore more efficient methods for the sensitive detection of E₂.

Photoelectrochemical (PEC) detection technology has been constantly studied for quantitative detection of various environmental targets given its low cost, simple instrumentation, and high sensitivity [8–10]. The aptamer recognition strategy has recently been widely used as a promising approach to capture target analytes in complex environmental mediums due to its good stability, simple modification, flexible sequence design, and so on [11–13]. Besides, the emerging self-powered devices have attracted widespread attention in various fields due to their superior energy saving and flexible usage in practice [14]. The proposed self-powered sensing platform primarily provides a promising application strategy for rapid on-site environmental detection [15, 16].

✉ Tao Yan
yantujn@163.com

¹ School of Water Conservancy and Environment, University of Jinan, Jinan 250022, People's Republic of China

² Shandong Academy of Environmental Science Co., Ltd, Jinan 250013, People's Republic of China

³ Key Laboratory of Interfacial Reaction & Sensing Analysis in Universities of Shandong, School of Chemistry and Chemical Engineering, University of Jinan, Jinan 250022, People's Republic of China

The photoactive materials with superior properties are critical for a prominent PEC-sensing platform. Metal–organic frameworks (MOFs) materials have been applied to fabricate an efficient photoactive matrix for modern PEC sensor construction [17–19]. Zirconium-based MOFs (UiO-66) that have become more and more attractive due to the metal center clusters (Zr–O) could greatly shorten the carrier transmission distance and improve the electron transfer rate, which remarkably enhances the photocatalytic performance of UiO-66 [20–22]. Meanwhile, metal doping could further facilitate the separation efficiency of photo-induced carriers due to forming abundant redox sites [23–26]. Many metals-doped UiO-66, including Cu–UiO-66 [23], Fe–UiO-66 [27] and Co/Zr–UiO-66 [28] have been developed for photocatalytic or photoelectrochemical application. Moreover, AgInS₂ is a ternary metal sulfide with a narrow direct band gap (1.87–2.03 eV) as well as a higher conduction band (CB) position [29, 30], which is generally acted as a photoactive material to boost the light absorption and facilitate the photogenerated electron transfer in photovoltaics and photocatalysis fields [31, 32]. Besides, carbon nanodots (CDs) are extensively used in establishing PEC-sensing platforms owing to their rapid electron transfer, excellent conductivity, and up-conversion photoluminescence [33–35]. For the construction of a self-powered PEC-sensing platform, AgInS₂ and CDs–modified UiO-66 photoelectrode is still lacking.

Herein, a novel AgInS₂@Co/Ni–UiO-66@CDs photoelectrode with excellent PEC performance was fabricated by a simple two-step preparation method. Then, a self-powered PEC aptasensor was constructed herein for E₂ detection on account of the obtained photoactive materials. The co-doped of Co and Ni markedly improved the photoelectrochemical activity of UiO-66, and the matched energy level of AgInS₂ and Co/Ni–UiO-66 promoted carrier mobility. Furthermore, the coupling of CDs further enhanced the conductivity and light absorption of the modified photoelectrode. Therefore, an increased anode-photocurrent signal was obtained in 0.0 V bias voltage. Furthermore, the specific E₂-aptamer was adopted as a target marking and recognition unit to facilitate the selectivity and sensitivity of the proposed aptasensor. In the detecting process, the specific recognition between E₂ and aptamer conducted to the conformational change of the aptamers and complete dissociation of some aptamers on the PEC-sensing interface, resulting in a raised photocurrent signal. The concentration of E₂ was quantified by counting the fluctuation of the anode-photocurrent signal.

Experimental

Materials and reagents

Zirconium tetrachloride (ZrCl₄, ≥ 98%), 2-aminoterephthalic acid (C₈H₇NO₄, ≥ 99%), and Indium trichloride

(InCl₃, ≥ 99.9%) were acquired from Macleans Chemical Technology Co., Ltd (Shanghai, China). N, N-dimethylformamide (C₃H₇NO, DMF, AR), silver nitrate (AgNO₃, AR), ascorbic acid (AA, AR), and sodium sulfide (Na₂S·9H₂O, AR) were acquired from Sinopharm Chemical Reagent Co., Ltd (Shanghai, China). Cobalt chloride (CoCl₂·6H₂O, ≥ 99.9%) was acquired from Tianjin Fuchen Chemical Reagent Factory (Tianjin, China). Estradiol (monoclonal antibody, standard sample) was acquired from Shenzhen Anti Industrial Technology Co., Ltd (Shenzhen, China).

Indium-tin-oxide (ITO) conductive glass was acquired from Zhuhai Kaiwei Electronic Components Co., Ltd (Zhuhai, China). Terminal aminated aptamer (5'-NH₂-GCT-TCC-AGC-TTA-TTG-AAT-TAC-ACG-CAG-AGG-GTA-GCG-GCT-CTG-CGC-ATT-CAA-TTG-CTG-CGC-GCT-GAA-GCG-CGG-AAG-C-3') was from Shanghai Shengong Biological Engineering Co., Ltd (Shanghai, China).

The other details have been represented in the *Electronic Supplementary Material* (ESM).

Apparatus

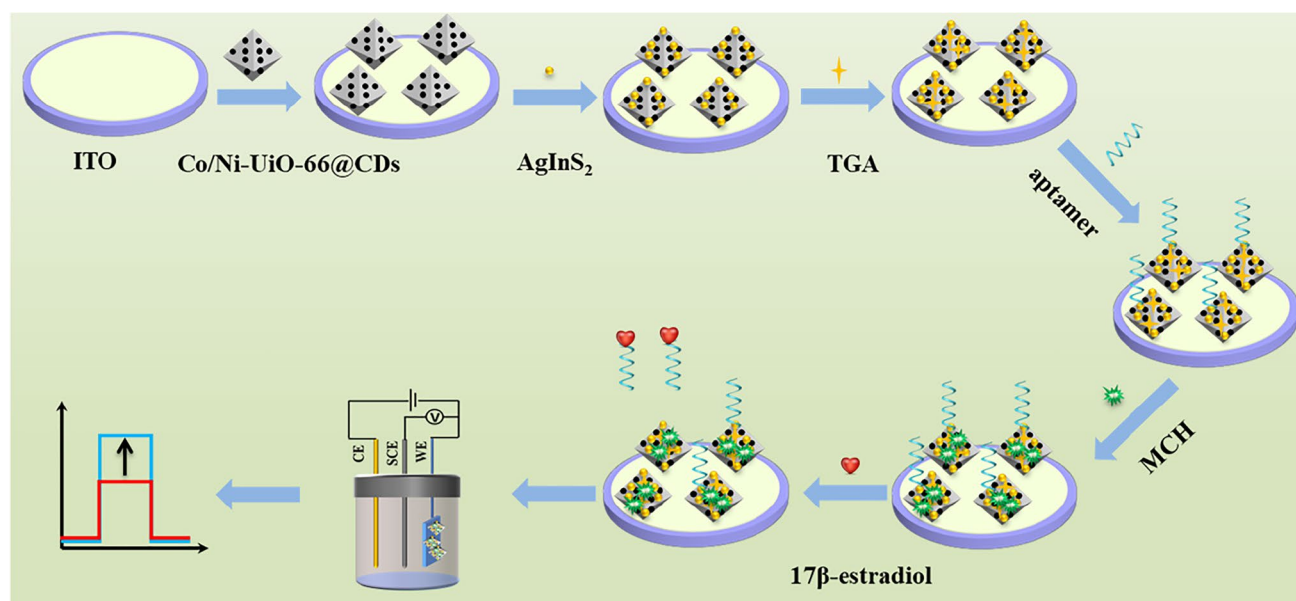
Photoelectrochemical workstation (PP211) was purchased from Zahner (Germany). UV–Visible spectrophotometer (lambda35) was purchased from Perkin-Elmer (USA). Ultraviolet–visible diffuse reflectance (UV-3101PC) was purchased from Shimadzu Corporation (Japan). The other details have been represented in the supplementary information.

Synthesis of Co/Ni–UiO-66@CDs

0.233 g of ZrCl₄ and 0.181 g of terephthalic acid were dissolved into 60 mL (400 rpm) of DMF solution in sequence at room temperature. Then, 0.065 g of CoCl₂·6H₂O and 0.064 g of NiCl₂·6H₂O were mixed and stirred for 60 min (600 rpm) at standard ambient temperature [36]. Then, a certain number of CDs, synthesized according to the literature [37] (details shown in supplementary information), were mixed into the above solution. The compound was placed in a Teflon-lined autoclave (100 mL capacity) and incubated at 120 °C for 48 h. Ultimately, the mixture was thoroughly cleaned with DMF (60 mL) and methanol (60 mL) and dried at 60 °C overnight.

Fabrication of AgInS₂@Co/Ni–UiO-66@CDs/ITO photoelectrode

Before preparing the modified electrode, indium-tin-oxide (ITO) substrates had been sliced in earnest into 2.0 × 0.5 cm²



Scheme 1 The fabrication process of the proposed PEC aptasensor

pieces. After that, the ITO slices were ultrasonically washed thrice with laundry detergent, acetone, and deionized water. These electrodes were dried naturally before use.

The Co/Ni-UiO-66@CDs suspension (10 μ L, 4 mg/L) was coated on the ITO electrode. Then, the Co/Ni-UiO-66@CDs/ITO electrode was immersed in 0.05 mol/L of InCl_3 ethanol solution for 30 s, followed by the Co/Ni-UiO-66@CDs/ITO electrode that was immersed in 0.1 mol/L $\text{Na}_2\text{S}\cdot 9\text{H}_2\text{O}$ solution for 30 s. Afterward, the Co/Ni-UiO-66@CDs/ITO electrode was flushed with methanol (10 mL) to purge away superfluous substances. Then, the obtained electrode was immersed in 0.05 mol/L AgNO_3 solution (10 mL), maintained for 120 min, and then thoroughly flushed with ultrapure water (10 mL) and ethanol (10 mL) multiple times. Consequently, the AgInS_2 @Co/Ni-UiO-66@CDs/ITO photoelectrode was fabricated and dried naturally before use.

Fabrication of self-powered PEC aptasensor

This AgInS_2 @Co/Ni-UiO-66@CDs/ITO electrode was soaked in 3 mmol/L thioglycolic acids (TGA) solution for approximately 20 min of touching off the assembly of carboxy (-COOH) groups. Subsequently, 5 μ L aptamer solution (2 μ mol/L) was coated on the AgInS_2 @Co/Ni-UiO-66@CDs/ITO photoelectrode (4 $^\circ\text{C}$, 1 h). Then, the obtained aptamer/TGA/ AgInS_2 @Co/Ni-UiO-66@CDs/ITO electrode was rinsed with some unbounded aptamers with phosphate buffer solution. Afterward, 10 μ L of 1 mmol/L 6-mercapto-1-hexanol (MCH) was incubated to cut off specific sites. And then, the electrodes were rinsed thoroughly with phosphate buffer solution. Next, E_2 solutions were dipped on the

MCH/aptamer/TGA/ AgInS_2 @Co/Ni-UiO-66@CDs/ITO electrodes (4 $^\circ\text{C}$, 30 min), then the resulting electrodes were washed thoroughly. Finally, the PEC aptasensor was accomplished. Scheme 1 showed the preparation of the proposed PEC aptasensor.

The PEC testing was conducted minutely at an electrochemical workstation using a conventional three-electrode system. The bias potential was 0.0 V. The light-emitting diode (LED) lamp ($\lambda > 450$ nm) was utilized as the irradiation source of visible light, and this light intensity was 180 W/cm^2 . The other particulars were presented in the supplementary information.

Results and discussion

Characterization of AgInS_2 @Co/Ni-UiO-66@CDs photoelectrode

The as-prepared AgInS_2 @Co/Ni-UiO-66@CDs were characterized by scanning electron microscopy (SEM) and transmission electron microscopy (TEM). Figure 1A showed that the pristine UiO-66 performed an agglomerated nanocrystal form. The doping of Co and Ni could regulate the UiO-66 morphology [38, 39]. After doping Co and Ni, the obtained Co/Ni-UiO-66 manifested a well-dispersive cubic morphology with precise edges (Figs. 1B and S1A). Figure 1C and D show that the rough surface of AgInS_2 @Co/Ni-UiO-66@CDs was distinguishable compared with that of Co/Ni-UiO-66. Figure 1D and E also exhibited that CDs and AgInS_2 were uniformly decorated on Co/Ni-UiO-66.

Fig. 1 SEM images of (A) UiO-66, (B) Co/Ni-UiO-66 and (C) AgInS₂@Co/Ni-UiO-66@CDs; TEM images of (D) AgInS₂@Co/Ni-UiO-66@CDs; HRTEM images of (E) AgInS₂@Co/Ni-UiO-66@CDs; (F) XRD pattern of (a) Co/Ni-UiO-66, (b) Co/Ni-UiO-66@CDs and (c) AgInS₂@Co/Ni-UiO-66@CDs

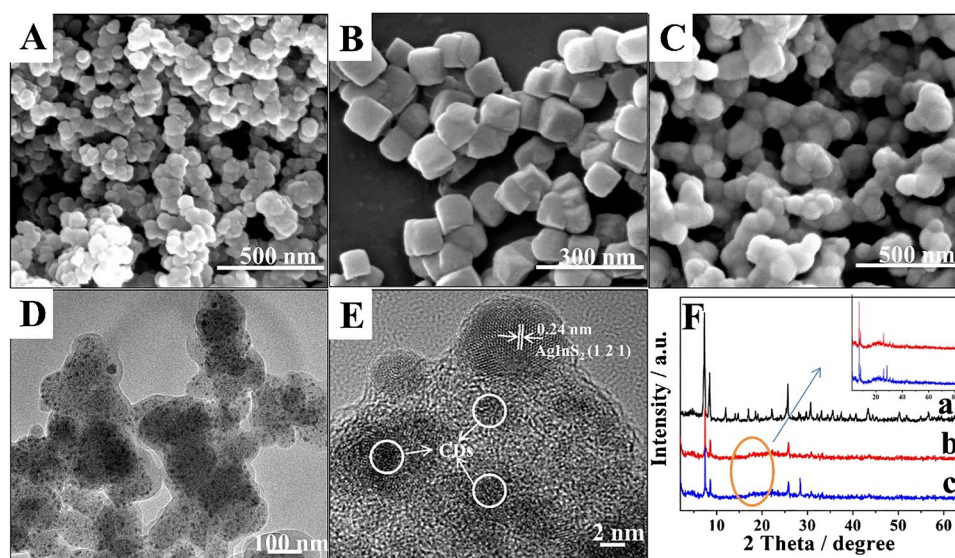


Figure 1E showed the high-resolution transmission electron microscopy (HRTEM) image of AgInS₂@Co/Ni-UiO-66@CDs, and the clear lattice fringes of $d=0.24$ nm corresponding to the (1 2 1) plan of AgInS₂, and the adopted CDs also could be revealed on the surface of Co/Ni-UiO-66 [40]. These results indicated that the photoactive material had been successfully assembled with a tight and compact heterojunction interface.

X-ray diffractometer (XRD) was utilized to investigate the crystalline phase of the AgInS₂@Co/Ni-UiO-66@CDs (Fig. 1F). There were no distinct peaks in the diffraction spectrum due to the small amounts and the excellent dispersion of Co and Ni, implying that the doping of Co and Ni couldn't transform the crystal phase structure of the UiO-66, which showed no difference from the previous literature [41]. Besides, compared with the pattern of Co/Ni-UiO-66, the spectral lines of Co/Ni-UiO-66@CDs showed a weak diffraction peak that occurred at 21°, indicating the successful doping of CDs [42]. Moreover, curve c presented a weak peak at around 28.4°, corresponding to the (1 2 1) plane of AgInS₂ (JCPDS 25–1328) [43, 44], indicating the successful doping of AgInS₂.

The optical absorption properties of AgInS₂@Co/Ni-UiO-66@CDs photoelectrode could be emerged by ultraviolet–visible diffuse-reflection spectra (UV–vis DRS) (Fig. S5A and B). As we can see, the absorption edge of Co/Ni-UiO-66 and AgInS₂ was about 350 and 600 nm, equivalent to the band gap energy of 3.50 eV and 2.03 eV, respectively. Furthermore, compared with Co/Ni-UiO-66, the absorption edge of AgInS₂@Co/Ni-UiO-66@CDs photoelectrode was red-shifted to the visible light region, bearing out the significant advance of the light-harvesting performance for AgInS₂@Co/Ni-UiO-66@CDs photoelectrode.

The Mott-Schottky (M-S) curves demonstrated the band structure of Co/Ni-UiO-66 and AgInS₂. As showed in Fig. S5C and D, the flat band potential (V_{fb}) of Co/Ni-UiO-66 and AgInS₂ were -0.8 eV (vs. SCE) and -0.84 eV (vs. SCE), in contrast, were equal to -0.56 eV (vs. NHE) and -0.60 eV (vs. NHE). As previously reported [36], the positive slope of the linear region indicated the AgInS₂, Co/Ni-UiO-66, had the properties of n-type semiconductors and the CB potential (E_{CB}) of n-type semiconductors was roughly 0.10–0.20 eV negative than the flat band potential. Consequently, the E_{CB} of Co/Ni-UiO-66 and AgInS₂ were approximately -0.66 eV and -0.70 eV (vs. NHE), respectively. According to above data, the valence band (VB) potential (E_{VB}) of Co/Ni-UiO-66 and AgInS₂ were estimated to be $+2.84$ eV and $+1.33$ eV (vs. NHE).

Detection mechanism

The electron-transfer mechanism is illustrated in Fig. 2A. As we can see, the E_{VB} and E_{CB} of AgInS₂ were higher than Co/Ni-UiO-66, and the photo-induced electrons were migrated from AgInS₂ to the CB of Co/Ni-UiO-66 when excited by visible light and then injected into ITO glass. In the meantime, the photoelectrons generated in the organic ligand of Co/Ni-UiO-66 could be transferred to the zirconium oxygen cluster to reduce Zr⁴⁺ to Zr³⁺ [45]. In addition, the photoelectrons could also reduce the oxidation states of Co³⁺ and Ni³⁺ to Co²⁺ and Ni²⁺, respectively. In contrast, the unstable states of Zr³⁺, Co²⁺, and Ni²⁺ were easily regenerated into respective oxidation states, further promoting the separation of photo-induced charges. Furthermore, the CDs had two functions: on the one side, CDs could act as electron conduction bridges, accelerating the electron transfer and separation. On the other side, CDs absorbed longer

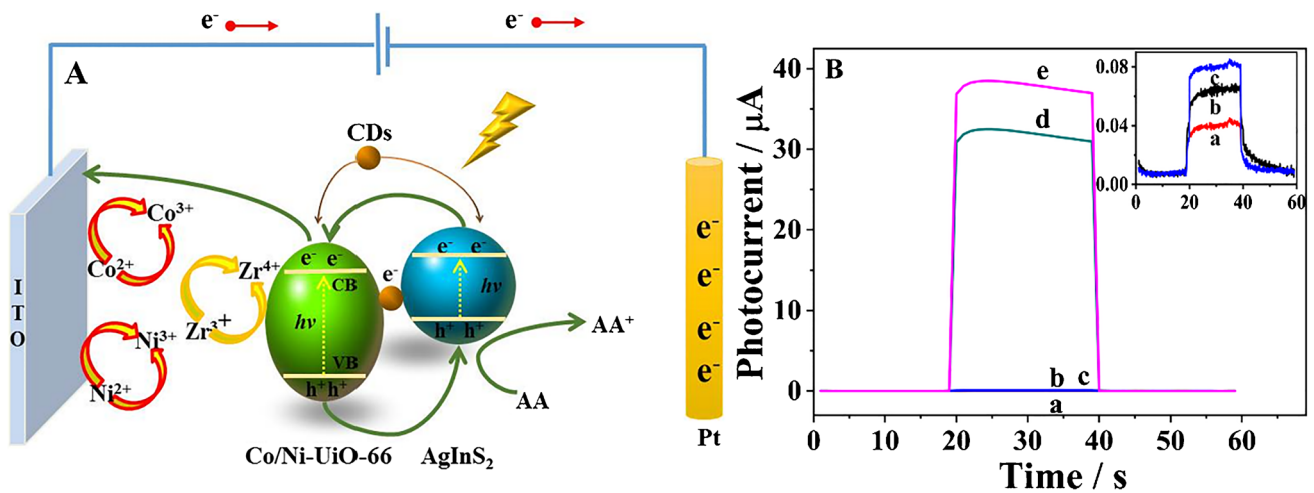


Fig. 2 (A) Schematic illustration of the photoelectrochemical aptasensor; (B) The transient photocurrent responses of (a) UiO-66, (b) Co/Ni-UiO-66/ITO, (c) Co/Ni-UiO-66@CDs/ITO, (d) AgInS₂@Co/Ni-UiO-66/ITO, (e) AgInS₂@Co/Ni-UiO-66@CDs/ITO

wavelength radiation and emitted 400–600 nm light [46], further improving light utilization. Moreover, the photogenerated holes were transferred from the VB of Co/Ni-UiO-66 to AgInS₂ and then captured by the AA.

Fig. 2B displayed the distinct photocurrent signals of the modified electrodes under visible light illumination. The photocurrent of Co/Ni-UiO-66 had been ameliorated (curve b) compared with UiO-66 (curve a). After the adoption of CDs, the photocurrent response was further enhanced (curve c). Distinguishably, with the modification of AgInS₂, the photocurrent was significantly improved (curve e), indicating that the appropriate energy level of AgInS₂ and Co/Ni-UiO-66 further restrained the recombination of carriers. Furthermore, when a precious number of CDs was incorporated, the AgInS₂@Co/Ni-UiO-66@CDs photoelectrode exhibited a higher photocurrent intensity than that of AgInS₂@Co/

Ni-UiO-66 (curve d), attributing to the superb electrical conductivity of CDs.

Characterization of the fabricated PEC aptasensor

The photo-induced interfacial charge transfer rate was studied by electrochemical impedance spectroscopy (EIS). The diameter of the semicircle in the high-frequency region represented figuratively the size of the resistance (R_{et}) [47]. As shown in Fig. 3A, for bare ITO electrodes, the semicircle in the impedance spectrum displayed a minimal diameter; as expected, the R_{et} value was the smallest (curve a). The R_{et} value increased with the modification of Co/Ni-UiO-66@CDs (curve b) and AgInS₂ (curve c). When the aptamer (curve d) and MCH (curve e) were deposited, R_{et} value further increased, demonstrating that the interface electron

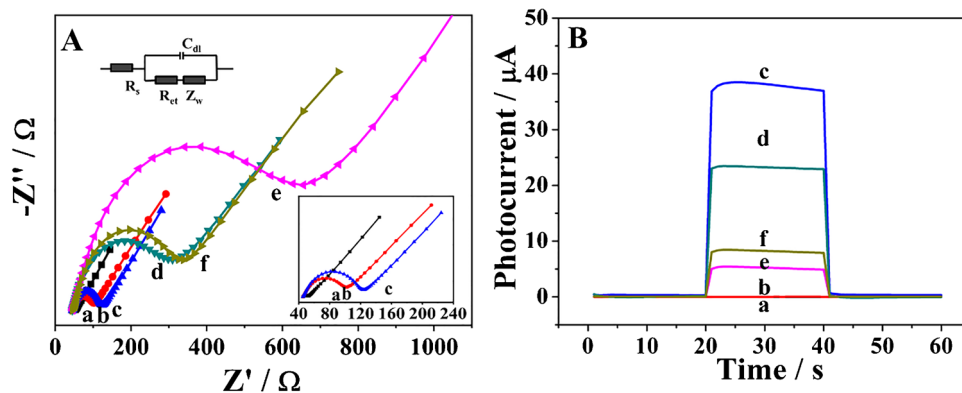


Fig. 3 (A) EIS (electrolyte: 2.5 mmol/L [Fe(CN)₆]^{3-/4-}) and (B) photocurrent responses of different modified electrode (electrolyte: 0.1 mol/L phosphate buffer solution, pH=7.4): (a) ITO, (b) Co/Ni-UiO-66@CDs/ITO, (c) AgInS₂@Co/Ni-UiO-66@CDs/ITO, (d)

aptamer/AgInS₂@Co/Ni-UiO-66@CDs/ITO, (e) MCH/aptamer/AgInS₂@Co/Ni-UiO-66@CDs/ITO, (f) E₂/MCH/aptamer/AgInS₂@Co/Ni-UiO-66@CDs/ITO

transfer was hindered. With the deposition of E_2 , the R_{et} value decreased (curve f) on the contrary. This was mainly due to the specific recognition reaction, contributing to the conformation of the aptamer to transform, shedding off some aptamers on the electrode interface [48].

Fig. 3B shows the photocurrent change during the layer-by-layer modification. The photocurrent of $AgInS_2@Co/Ni-UiO-66@CDs/ITO$ photoelectrode reached the maximum. With the improvement of the E_2 -aptamer and the blocking of MCH, the photocurrent decreased by degrees. The results revealed that modifying the substances mentioned above hindered the transfer of electrons and the capture of holes. However, when E_2 was caught catching by the aptamer/ $TGA/AgInS_2@Co/Ni-UiO-66@CDs/ITO$, a remarkable enhancement in photocurrent was discerned due to the aptamer bound to E_2 falling off from the electrode. This result indicated the successful modification of the layers of electrodes.

Optimization of experimental condition

Fig. S6A revealed different effects of CDs with various mass fractions on the $Co/Ni-UiO-66@CDs/ITO$ electrode photocurrent. As the mass fraction of CDs raised, photocurrent gradually increased. However, the photocurrent decreased as the mass fraction of CDs further extended. Therefore, the best mass percentage of CDs was 5%. Moreover, the modification of $AgInS_2$ could be proven to influence the anode-photocurrent intensity. As shown in Figs S6B and S6C, when the number of modified layers was 10 and the immersion time of silver nitrate was 120 min, the photocurrent reached its peak value. Besides, the soaking time caused the photocurrent intensity to decrease. And the results revealed that more redundant heterojunction interfaces could be led due to the excessive $AgInS_2$, inhibiting the photoelectron transfer. When the applied bias voltage varied from -0.2 V to 0.0 V, as revealed in Fig. S6D, the photocurrent gradually increased and attained its maximum value at

0.0 V. Along with external bias voltage was greater than 0.0 V, the photocurrent dwindled, which might be attributed to the higher the applied bias, the more severe damage to the modified electrode surface. Therefore, the steady anode-photocurrent signal output without an external power supply provides a reliable photoelectric translating platform for the self-powered PEC aptasensor construction.

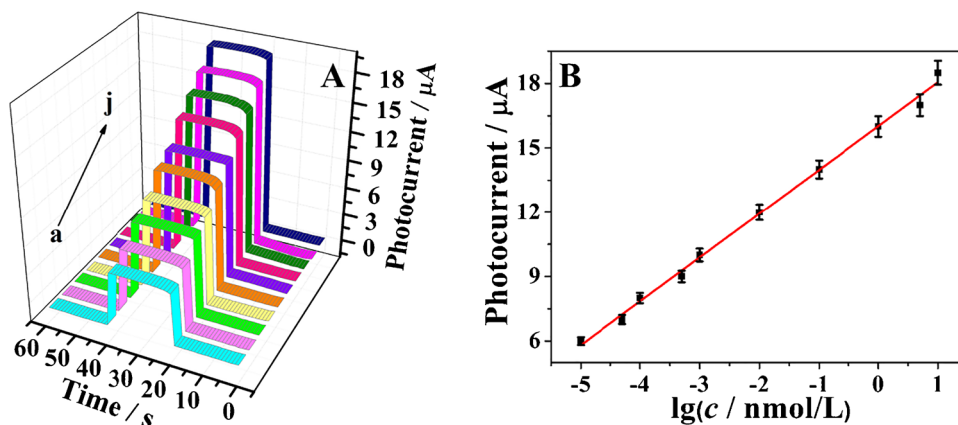
PEC aptasensor for E_2 detection

Fig. 4A showed the photocurrent intensity when distinct concentrations of E_2 were gauged through the self-powered PEC aptasensor. The concentration range of E_2 was 10 fmol/L– 10 nmol/L. As the consistence of E_2 raised by degrees, the photocurrent gradually increased. That was probably owing to aptamer dissociating from the electrode surface. Further, observation showed a fine linear relationship between enhancement of the photocurrent and logarithm of the E_2 concentration from Fig. 4B. The calibration curve equation was $I = 16 + 2.04 \lg c$, the correlation coefficient was 0.996 , and the detection limit was lower than 3 fmol/L ($S/N = 3$). Contrasting with a majority of previously reported detection methods, the self-powered PEC aptasensor as-prepared possessed one acceptable response range and a lower detection limit (Table S1).

Selectivity, stability, and reproducibility

Under continuous detection, Fig. S7A showed the stability of the PEC aptasensor. The sensing platform worked for 400 s under the on/off cycle, and the photocurrent signal had no significant change, demonstrating that the designed self-powered PEC aptasensor could possess excellent stability to detect E_2 . Five representative endocrine disruptors (estriol, bisphenol A, Ethinyl E_2 , diethylstilbestrol and 4-nonylphenol) were opted as interfering species for interference tests. As shown in Fig. S7B, adding different endocrine disruptors with a more than 100-fold concentration to five parts of E_2

Fig. 4 (A) The photocurrent responses (electrolyte: 0.1 mol/L phosphate buffer solution, $pH = 7.4$) of the PEC aptasensor at different E_2 concentrations (1.0×10^{-5} – 10 nmol/L); (B) Logarithmic calibration curve of different E_2 concentrations



solution, respectively. These interfering substances had no noticeable effect on the photocurrent signal, indicating that the obtained self-powered PEC aptasensor possessed high anti-interference ability.

The reproducibility of the self-powered PEC aptasensor was demonstrated in Fig. S7C. Five different E_2 /MCH/aptamer/AgInS₂@Co/Ni-UiO-66@CDs/ITO electrodes were modified similarly with 100 fmol/L E_2 solutions, and the tested result exhibited the relative standard deviation (RSD) of photocurrent is 2.5%. The results reflected satisfactory photocurrent response and reproducibility of the PEC aptasensor. In addition, the storage stability of the proposed sensor was evaluated by storing the PEC aptasensor at 4 °C for 8 and 14 days in Fig. S7D. 95% and 92% of the initial photocurrent intensity were obtained to detect E_2 (100 fmol/L), indicating its excellent storage stability.

Real sample analysis

The self-powered PEC aptasensor–analyzed E_2 in actual water samples. The samples were from the Jiazi River (Jinan, China). Before analysis, the water samples were filtered through a 0.22 μm membrane to get rid of suspended solids. Then, the actual water samples were tested by the standard addition method, and the results were shown in Table S2. The standard solution of E_2 with the concentration of 1.0, 5.0, and 10.0 nmol/L was added to the water sample, and the obtained RSD was 3.3%, 3.2%, and 1.9%, the recovery was 101%, 100%, and 99.5%. The satisfied results indicated that the designed aptasensing platform had a promising application prospect for E_2 detection in actual water. However, the self-powered PEC aptasensor couldn't be used in mass production because the preparation technology is not mature enough, and they are mainly used in scientific research. Even so, there is no doubt that the constructed aptasensor still has excellent potential in actual sample detection, indicating a broader application prospect.

Conclusions

In general, a novel self-powered aptasensing platform has been successfully established for the sensitive detection of E_2 based on the AgInS₂@Co/Ni-UiO-66@CDs photoelectrode. The well-designed photoelectrode greatly amplified the signal strength of anode-photocurrent without bias voltage, which provides a reliable photoelectric translating platform for the self-powered PEC aptasensor. The specific recognition between E_2 and aptamer resulted in a raised photocurrent signal, and the concentration of E_2 was quantified by counting the fluctuation of anode-photocurrent signal. On this basis, the proposed self-powered aptasensor showed high selectivity, stability, and acceptable reproducibility.

This work provided a promising platform for E_2 detection in actual water samples and also widened the design ideas of PEC device for ultra-sensitive environmental analysis.

Supplementary Information The online version contains supplementary material available at <https://doi.org/10.1007/s00604-022-05409-z>.

Funding This study was supported by the National Key Scientific Instrument and Equipment Development Project of China (No. 21627809), National Natural Science Foundation of China (No. 21777056), Natural Science Foundation of Shandong Province (Nos. ZR2020MB091, ZR2020MB037). Youth Innovative Talents Recruitment and Cultivation Program of Shandong Higher Education. Jinan Scientific Research Leader Workshop Project (2018GXRC021).

Declarations

Conflict of interest The authors declare no competing interests.

References

1. Yao X-L, Wang Z-H, Zhao M, Liu S-J, Su L-H, Dou L-N, Li T, Wang J-L, Zhang D-H (2021) Graphite-like carbon nitride-laden gold nanoparticles as signal amplification label for highly sensitive lateral flow immunoassay of 17β-estradiol. *Food Chem* 347:129001. <https://doi.org/10.1016/j.foodchem.2021.129001>
2. Ming W-N, Wang X-Y, Lu W-H, Zhang Z, Song X-L, Li J-H, Chen L-X (2017) Magnetic molecularly imprinted polymers for the fluorescent detection of trace 17β-estradiol in environmental water. *Sens Actuators, B Chem* 238:1309–1315. <https://doi.org/10.1016/j.snb.2016.09.111>
3. Tian X, Song H-J, Wang Y, Tian X-M, Tang Y-H, Gao R-X, Zhang C-X (2020) Hydrophilic magnetic molecularly imprinted nanobeads for efficient enrichment and high performance liquid chromatographic detection of 17β-estradiol in environmental water samples. *Talanta* 220:121367. <https://doi.org/10.1016/j.talanta.2020.121367>
4. Wang R, Chon H, Lee S, Cheng Z, Hong S-H, Yoon Y-H, Choo J (2016) Highly sensitive detection of hormone estradiol E_2 using SERS-based immunoassays for the clinical diagnosis of precocious puberty. *ACS Applied Materials & Interfaces* 8(17):10665–10672
5. Zhao Z, Chen H, Cheng Y, Huang Z-Y, Wei X-H, Feng J-L, Cheng J, Mugo S-M, Nicole J-R, Guo Z-Z (2022) Electrochemical aptasensor based on electrodeposited poly(3,4-ethylenedioxythiophene)-graphene oxide coupled with Au@Pt nanocrystals for the detection of 17β-estradiol. *Microchim Acta* 189:178. <https://doi.org/10.1007/s00604-022-05274-w>
6. Yang H, Xu D-K (2022) Highly-sensitive and simple fluorescent aptasensor for 17 β-estradiol detection coupled with HCR-HRP structure. *Talanta* 240:123094. <https://doi.org/10.1016/j.talanta.2021.123094>
7. Yan T, Wu T-T, Wei S-Y, Wang H-Q, Sun M, Yan L-G, Wei Q, Ju H-X (2020) Photoelectrochemical competitive immunosensor for 17β-estradiol detection based on ZnIn₂S₄@NH₂-MIL-125(Ti) amplified by PDA NS/Mn: ZnCdS. *Biosens Bioelectron* 148:111739. <https://doi.org/10.1016/j.bios.2019.111739>
8. Bukkitgar S-D, Shetti N-P, Aminabhavi T-M (2021) Electrochemical investigations for COVID-19 detection-a comparison with other viral detection methods. *Chem Eng J* 420:127575. <https://doi.org/10.1016/j.cej.2020.127575>

- Wang Z-W, Wang H, Zeng Z-T, Zeng G-M, Xu P, Xiao R, Huang D-L, Chen X-J, He L-W, Zhou C-Y, Yang Y, Wang Z-X, Wang W-J, Xiong W-P (2020) Metal-organic frameworks derived $\text{Bi}_2\text{O}_2\text{CO}_3/\text{porous carbon nitride}$: a nanosized Z-scheme systems with enhanced photocatalytic activity. *Appl Catal B* 267:118700. <https://doi.org/10.1016/j.apcatb.2020.118700>
- Deng Y, Yan W-J, Guo Y-J, Wang Q, Bi Y-P, Dong C, Fan L-F (2022) Highly sensitive and selective photoelectrochemical aptasensing of di-2-ethylhexyl phthalate based on graphene quantum dots decorated TiO_2 nanotube arrays. *J Hazard Mater* 426:128107. <https://doi.org/10.1016/j.jhazmat.2021.128107>
- Wen Z-R, Zhu W-R, You F-H, Yuan R-S, Ding L-J, Hao N, Wei J, Wang K (2022) Ultrasensitive photoelectrochemical aptasensor for carbendazim detection based on in-situ constructing Schottky junction via photoreducing Pd nanoparticles onto CdS microsphere. *Biosens Bioelectron* 203:114036. <https://doi.org/10.1016/j.bios.2022.114036>
- Hao X-F, Guan Y, Liu F, Zhang Y-J, Zhai Y-J, Niu L-M (2022) Ultrasensitive detection and application of estradiol based on nucleic acid aptamer and circulating amplification technology. *J Electroanal Chem* 913:116284. <https://doi.org/10.1016/j.jelechem.2022.116284>
- Tu L-H, Zhu J-H, Tanjung A-P, Wang M, Kang J-W, Wang A-J, Mei L-P, Xue Y-D, Song P (2022) A signal-off photoelectrochemical aptasensor for ultrasensitive 17β -estradiol detection based on rose-like CdS@C nanostructure and enzymatic amplification. *Microchim Acta* 189:56. <https://doi.org/10.1007/s00604-022-05164-1>
- Sun J, He Y-H, He S, Liu D-Q, Lu K-N, Yao W-Q, Jia N-Q (2022) A self-powered photoelectrochemical cathodic molecular imprinting sensor based on Au@ TiO_2 nanorods photoanode and Cu_2O photocathode for sensitive detection of sarcosine. *Biosens Bioelectron* 204:114056. <https://doi.org/10.1016/j.bios.2022.114056>
- Huang T-X, Li C-P, Liang D-D, Li S-R, Zhou H, Ge P, Zhu X-D, Liu T-F (2022) Metal-organic frameworks-based hierarchical heterojunction coupling with plasmonic nanoshells for self-powered photoelectrochemical immunoassay. *Chem Eng J* 431:133465. <https://doi.org/10.1016/j.cej.2021.133465>
- Yang X-X, Qu L-H, Gao F, Hu Y-X, Yu H, Wang Y-X, Cui M-Q, Zhang Y-X, Fu Z-D, Huang Y-W, Feng W, Li B, Hu P-A (2022) High-performance broadband photoelectrochemical photodetectors based on ultrathin $\text{Bi}_2\text{O}_2\text{S}$ nanosheets. *ACS Appl Mater Interfaces* 14:7175–7183. <https://doi.org/10.1021/acsami.1c22448>
- Yoon J-W, Kim D-H, Kim J-H, Jang H-W, Lee J-H (2019) NH_2 -MIL-125(Ti)/ TiO_2 nanorod heterojunction photoanodes for efficient photoelectrochemical water splitting. *Appl Catal B* 244:511–518. <https://doi.org/10.1016/j.apcatb.2018.11.057>
- Cao W, Yuan Y-H, Yang C, Wu S-C, Cheng J-H (2020) In-situ fabrication of $g\text{-C}_3\text{N}_4/\text{MIL-68(In)-NH}_2$ heterojunction composites with enhanced visible-light photocatalytic activity for degradation of ibuprofen. *Chem Eng J* 391:123608. <https://doi.org/10.1016/j.cej.2019.123608>
- Pan Y, Yuan X-Z, Jiang L-B, Wang H, Yu H-B, Zhang J (2020) Stable self-assembly AgI/ $\text{UiO-66(NH}_2\text{)}$ heterojunction as efficient visible light responsive photocatalyst for tetracycline degradation and mechanism insight. *Chem Eng J* 384:123310. <https://doi.org/10.1016/j.cej.2019.123310>
- Xiao K, Meng L-X, Du C-C, Zhang Q-Q, Yu Q, Zhang X-H, Chen J-H (2021) A label-free photoelectrochemical biosensor with near-zero-background noise for protein kinase a activity assay based on porous ZrO_2/CdS octahedra. *Sens Actuators, B Chem* 328:129096. <https://doi.org/10.1016/j.snb.2020.129096>
- Winaeta J, Shan B, McIntyre S-M, Ye L, Wang C, Liu J-C, Mu B (2020) A decade of UiO-66 research: a historic review of dynamic structure, synthesis mechanisms, and characterization techniques of an archetypal Metal-Organic Framework. *Crystal Growth Design* 20:1347–1362. <https://doi.org/10.1021/acs.cgd.9b00955>
- Wang Z-H, Yan Z-Y, Wang F, Cai J-B, Guo L, Su J-K, Liu Y (2017) Highly sensitive photoelectrochemical biosensor for kinase activity detection and inhibition based on the surface defect recognition and multiple signal amplification of metal-organic frameworks. *Biosens Bioelectron* 97:107–114. <https://doi.org/10.1016/j.bios.2017.05.011>
- Yin L-M, Wang D-B, Li X-P, He Y-Y, Liu X-Q, Xu Y-Y, Chen H (2022) One-pot synthesis of oxygen-vacancy-rich Cu-doped UiO-66 for collaborative adsorption and photocatalytic degradation of ciprofloxacin. *Sci Total Environ* 815:151962. <https://doi.org/10.1016/j.scitotenv.2021.151962>
- Kannan K, Radhika D, Reddy K-R, Raghu A-V, Sadasivuni K-K, Palani G, Gurushankar K (2021) Gd^{3+} and Y^{3+} co-doped mixed metal oxide nanohybrids for photocatalytic and antibacterial applications. *Nano Express* 2:010014. <https://doi.org/10.1088/2632-959X/abdd87>
- Kumar S, Reddy K-R, Reddy C-V, Shetti N-P, Sadhu V, Shankar M-V, Reddy V-G, Raghu A-V, Aminabhavi T-M (2021) Metal nitrides and graphitic carbon nitrides as novel photocatalysts for hydrogen production and environmental remediation. *Nanostructured Materials for Environmental Applications* 19:485. https://doi.org/10.1007/978-3-030-72076-6_19
- Reddy K-R, Jyothi M-S, Raghu A-V, Sadhu V, Naveen S, Aminabhavi T-M (2020) Nanocarbons-supported and polymers supported titanium dioxide nanostructures as efficient photocatalysts for remediation of contaminated wastewater and hydrogen production. *Nanophotocatalysis and Environmental Applications* 6:139. https://doi.org/10.1007/978-3-030-12619-3_6
- Guan Z-Y, Zhu S-B, Ding S, Xia D-S, Li D-Y (2022) Fe-O-Zr in MOF for effective photo-fenton bisphenol a degradation: boosting mechanism of electronic transmission. *Chemosphere* 299:134481. <https://doi.org/10.1016/j.chemosphere.2022.134481>
- Kong X-X, Pan Q-Q, Song S, He Z-Q, Zeng T, Yu Y (2021) Dual metal UiO -type metal-organic frameworks for solar-driven photocatalytic hydrogen evolution. *The Journal of Physical Chemistry C* 125:20320–20330. <https://doi.org/10.1021/acs.jpcc.1c05866>
- Li H, Song W-Z, Cui X-Q, Li Y-H, Hou B-R, Zhang X-P, Wang Y-Q, Cheng L-J, Zhang P-F, Li J-R (2020) AgInS_2 and graphene co-sensitized TiO_2 photoanodes for photocathodic protection of Q235 carbon steel under visible light. *Nanotechnology* 31:305704. <https://doi.org/10.1088/1361-6528/ab85eb>
- Kowalik P, Mucha S-G, Matczyszyn K, Bujak P, Mazur L-M, Ostrowski A, Kmita A, Gajewska M, Pron A (2021) Heterogeneity induced dual luminescence properties of AgInS_2 and $\text{AgInS}_2\text{-ZnS}$ alloyed nanocrystals. *Inorganic Chemistry Frontiers* 8:3450. <https://doi.org/10.1039/d1qi00566a>
- Fu Y, Xiao K, Zhang X-H, Du C-C, Chen J-H (2021) Peptide cleavage-mediated and environmentally friendly photocurrent polarity switching system for prostate-specific antigen assay. *Anal Chem* 93:1076–1083. <https://doi.org/10.1021/acs.analchem.0c04086>
- Martinez M-N, Bajorowicz B, Klimczuk T, Zak A, Luczak J, Lisowski W, Medynska A-Z (2020) Synergy between AgInS_2 quantum dots and ZnO nanopyrramids for photocatalytic hydrogen evolution and phenol degradation. *J Hazard Mater* 398:123250. <https://doi.org/10.1016/j.jhazmat.2020.123250>
- Li B-L, Zhao S-J, Huang L, Wang Q, Xiao J-F, Lan M-H (2021) Recent advances and prospects of carbon dots in phototherapy. *Chem Eng J* 408:127245. <https://doi.org/10.1016/j.cej.2020.127245>
- Zhang X, Dong H, Sun X-J, Yang D-D, Sheng J-L, Tang H-L, Meng X-B, Zang F-M (2018) Step-by-step improving photocatalytic hydrogen evolution activity of $\text{NH}_2\text{-UiO-66}$ by constructing heterojunction and encapsulating carbon nanodots. *ACS Sustainable Chemistry Engineering* 6:11563–11569. <https://doi.org/10.1021/acssuschemeng.8b01740>
- Miao X-L, Yue X-Y, Ji Z-Y, Shen X-P, Zhou H, Liu M-M, Xu K-Q, Zhu J, Zhu G-X, Kong L-R, Shah S-A (2018) Nitrogen-doped

- carbon dots decorated on g-C₃N₄/Ag₃PO₄ photocatalyst with improved visible light photocatalytic activity and mechanism insight. *Appl Catal B* 227:459–469. <https://doi.org/10.1016/j.apcatb.2018.01.057>
36. Cao J, Yang Z-H, Xiong W-P, Zhou Y-Y, Peng Y-R, Li X, Zhou C-Y, Xu R, Zhansg Y-R (2018) One-step synthesis of Co-doped UiO-66 nanoparticle with enhanced removal efficiency of tetracycline: simultaneous adsorption and photocatalysis. *Chemical Engineering Journal* 353: <https://doi.org/10.1016/j.cej.2018.07.060>
37. Xu X-Y, Yan B (2016) Fabrication and application of a ratiometric and colorimetric fluorescent probe for Hg²⁺ based on dual-emissive metal-organic framework hybrids with carbon dots and Eu³⁺. *Journal of Materials Chemistry C* 4:1543. <https://doi.org/10.1039/c5tc04002g>
38. Li L-S, Pan X-B, Lan D-P, Xu H-T, Ge J-P, Zheng H-Q, Zheng Z-Z, Liu J-C, Xu Z-L, Liu J-K (2021) Etching of cubic Pd@Pt in UiO-66 to obtain nanocages for enhancing CO₂ hydrogenation. *Materials Today Energy* 19:100585. <https://doi.org/10.1016/j.mtener.2020.100585>
39. Guan Q-Q, Wang B, Chai X-S, Liu J, Gu J-J, Ning P (2017) Comparison of Pd-UiO-66 and Pd-UiO-66-NH₂ catalysts performance for phenol hydrogenation in aqueous medium. *Fuel* 205:130–141. <https://doi.org/10.1016/j.fuel.2017.05.029>
40. Zhang H, Zhao L-X, Geng F-L, Gao L-H, Wan B, Yang Y (2016) Carbon dots decorated graphitic carbon nitride as an efficient metal-free photocatalyst for phenol degradation. *Appl Catal B* 180:656–662. <https://doi.org/10.1016/j.apcatb.2015.06.056>
41. Charles V, Yang Y, Yuan M-L, Zhang J-T, Li Y-L, Zhang J-X, Zhao T-K, Liu Z-J, Li B, Zhang G-J (2021) CoO_x/UiO-66 and NiO/UiO-66 heterostructures with UiO-66 frameworks for enhanced oxygen evolution reactions. *New J Chem* 45:14822–14830. <https://doi.org/10.1039/d1nj01995c>
42. Xu Y, Yu H-M, Chudal L, Pandey N-K, Amador E-H, Bui B, Wang L-Y, Ma X-D, Deng S-P, Zhu X-H, Wang S-Y, Chen W (2021) Striking luminescence phenomena of carbon dots and their applications as a double ratiometric fluorescence probes for H₂S detection. *Materials Today Physics* 17:100328. <https://doi.org/10.1016/j.mtphys.2020.100328>
43. Zhang M-M, Li X-Y, Zhao Q-D, Fan S-Y, Jiang Z, Chen G-H (2017) AgInS₂ nanoparticles modified TiO₂ nanotube array electrodes: ultrasonic-assisted SILAR preparation and mechanism of enhanced photoelectrocatalytic activity. *Molecular Catalysis* 442:97–106. <https://doi.org/10.1016/j.mcat.2017.09.009>
44. Tsai H, Shaya J, Tesana S, Golovko V-B, Wang S-Y, Liao Y-Y, Lu C-S, Chen C-C (2020) Visible-light driven photocatalytic degradation of pirimicarb by Pt-doped AgInS₂ nanoparticles. *Catalysts* 10:857. <https://doi.org/10.3390/catal10080857>
45. Shi X-L, Zou J, Chen Z-G (2020) Advanced thermoelectric design: from materials and structures to devices. *Chem Rev* 120:7399–7515. <https://doi.org/10.1021/acs.chemrev.0c00026>
46. Huang X-N, Yang L-B, Hao S, Zheng B-Z, Yan L, Qu F-L, Asiri A-M, Sun X-P (2017) N-doped carbon dots: a metal-free co-catalyst on hematite nanorod arrays toward efficient photoelectrochemical water oxidation. *Inorganic Chemistry Frontiers* 4:537–540. <https://doi.org/10.1039/c6qi00517a>
47. Moradighadi N, Nestic S, Tribollet B (2021) Identifying the dominant electrochemical reaction in electrochemical impedance spectroscopy. *Electrochim Acta* 400:139460. <https://doi.org/10.1016/j.electacta.2021.139460>
48. Du X-X, Dai L-M, Jiang D, Li H-A, Hao N, You T-Y, Mao H-P, Wang K (2017) Gold nanorods plasmon-enhanced photoelectrochemical aptasensing based on hematite/N-doped graphene films for ultrasensitive analysis of 17β-estradiol. *Biosens Bioelectron* 91:706–713. <https://doi.org/10.1016/j.bios.2017.01.034>

Publisher's note Springer Nature remains neutral with regard to jurisdictional claims in published maps and institutional affiliations.

Springer Nature or its licensor holds exclusive rights to this article under a publishing agreement with the author(s) or other rightsholder(s); author self-archiving of the accepted manuscript version of this article is solely governed by the terms of such publishing agreement and applicable law.